Research Article

PCA-Aided Linear Precoding in Massive MIMO Systems with Imperfect CSI

Van-Khoi Dinh ⓘ,[1] **Minh-Tuan Le,**[2] **Vu-Duc Ngo,**[3] **and Chi-Hieu Ta**[1]

[1]*Le Quy Don Technical University, Hanoi, Vietnam*
[2]*MobiFone R&D Center, MobiFone Corporation, Hanoi, Vietnam*
[3]*Hanoi University of Science and Technology, Hanoi, Vietnam*

Correspondence should be addressed to Van-Khoi Dinh; vankhoi.tcu@gmail.com

In this paper, a low-complexity linear precoding algorithm based on the principal component analysis technique in combination with the conventional linear precoders, called Principal Component Analysis Linear Precoder (PCA-LP), is proposed for massive MIMO systems. The proposed precoder consists of two components: the first one minimizes the interferences among neighboring users and the second one improves the system performance by utilizing the Principal Component Analysis (PCA) technique. Numerical and simulation results show that the proposed precoder has remarkably lower computational complexity than its low-complexity lattice reduction-aided regularized block diagonalization using zero forcing precoding (LC-RBD-LR-ZF) and lower computational complexity than the PCA-aided Minimum Mean Square Error combination with Block Diagonalization (PCA-MMSE-BD) counterparts while its bit error rate (BER) performance is comparable to those of the LC-RBD-LR-ZF and PCA-MMSE-BD ones.

1. Introduction

In order to combat fading phenomenon in wireless communication, the Multiple-Input Multiple-Output (MIMO) technique has been proposed and already applied in 4th generation (4G) cellular networks [1]. The MIMO systems can significantly improve the channel capacity, the BER performance, and the reliability of wireless systems by increasing the number of antennas at both transmitter and receiver sides. The signal processing techniques for the uplink and downlink of both single-user MIMO, i.e., point-to-point MIMO, and multiuser MIMO (MU-MIMO) systems have been extensively researched in recent years. However, in practice, the number of antennas at the base sStation (BS) side in the MU-MIMO system is limited (normally fewer than 10) [2]. Therefore, the spectrum efficiency and system capacity are still relatively modest.

In order to cope with these issues, Massive MIMO systems have recently been proposed [1, 3–5]. In the Massive MIMO, the number of antennas at the BS can be up to hundreds (or even thousands) to simultaneously serve dozens of users using the same frequency resource. By increasing the number of antennas at the BS side, the Massive MIMO systems can significantly improve the channel capacity and enhance the spectrum utilization efficiency and the BER performance of the system [4]. However, the Massive MIMO systems also face many challenges such as hardware complexity, power consumption, and system cost due to a large number of antennas deployed at the BS [1, 2]. Basically, the Massive MIMO system can work in Time Division Duplex (TDD) or Frequency Division Duplex (FDD) mode. However, the TDD operation is preferable to the FDD operation because the TDD system can increase the number of antennas at the BS side to expand the system capacity without being affected by the coherence interval [1]. It is expected that Massive MIMO will be a key and bright candidate for the next generation wireless networks (e.g., 5G network) [1, 4, 6].

Undoubtedly, the Massive MIMO systems will become more complex as the number of antennas at the BS side gets very large. Therefore, reducing the complexities of the signal processing algorithms for both uplink and downlink in Massive MIMO systems is necessary. In Massive MIMO systems, the complex signal processing is performed at the BS side. Therefore, the precoding algorithms with low complexity, such as Zero Forcing (ZF), Minimum Mean Square Error (MMSE), and Maximum Ratio Transmission (MRT), are considered as suitable solutions for the downlink in the Massive MIMO system [7–9]. Besides, to eliminate interference from neighboring users and hence improve the system performance, the Block Diagonalization algorithm is adopted [10]. However, the computational complexity of the BD algorithm is very high. In this context, there exist different proposals to reduce the computational complexity based on the BD algorithm. For example, the QR decomposition based on Block Diagonalization (QR-BD) algorithm and the Pseudoinverse Block Diagonalization (PINV-BD) algorithms are proposed in [11, 12]. Nevertheless, the application of these algorithms to Massive MIMO systems remains a challenge task due to their excessive complexities.

In [13], Wang et al. proposed the precoder consisting of two components that utilize the LQ decomposition and Singular Value Decomposition (SVD) of the channel matrix. Based on the proposed approach in [14], in [15], the authors proposed the low-complexity Lattice Reduction- (LR-) aided precoding algorithms for the MU-MIMO system, referred to as LC-RBD-LR-ZF and LCR-BD-LR-MMSE. In the LC-RBD-LR-ZF and LC-RBD-LR-MMSE algorithms, the first precoding matrix is created by applying the QR decomposition to the extended channel matrix. The second precoding matrix is obtained using the conventional ZF and MMSE precoding algorithms in combination with the LR technique to provide the corresponding LC-RBD-LR-ZF and LC-RBD-LR-MMSE precoders. It was shown in [15] that the precoders significantly improved the system performance while reducing the computational complexity when compared to the one in [14]. In [16], the authors proposed a low-complexity linear precoding scheme for MU-MIMO systems based on the principal component analysis technique. However, the computational complexities of the precoders in [13–16] are still very high due to the QR and LQ decomposition operations. Therefore, these algorithms could hardly be applied to the Massive MIMO systems. Moreover, the systems are investigated under the assumption that the perfect channel state information (CSI) is available at the BS side.

Based on the principal component analysis technique and the linear precoding algorithms, the paper proposes a low-complexity precoder for Massive MIMO systems. In our proposed method, the precoding matrix is designed to consist two components. The first one is created by the MMSE precoding algorithm to minimize the interferences among neighboring users. The second one is designed based on the principal component analysis technique to improve the system performance. Numerical and simulation results show that the proposed precoder has remarkably lower computational complexity than the LC-RBD-LR-ZF in [15]

and lower computational complexity than the PCA-MMSE-BD in [16], while its BER performance is comparable to those of the LC-RBD-LR-ZF and PCA-MMSE-BD precoders in both perfect and imperfect CSI scenarios. In addition, simulation results show that the channel estimation error adversely affects the system performance no matter which precoder is adopted. The system performance decreases as the channel estimation error increases and vice versa for all precoders.

The rest of this paper is organized as follows. In Section 2, we present the Massive MIMO system model with imperfect CSI. The principal component analysis technique is reviewed in Section 3. In Section 4, we propose the linear precoding algorithm for the Massive MIMO systems that adopts the principal component analysis technique. Simulation results are shown in Section 5. Finally, conclusions are drawn in Section 6.

1.1. Notation. The notations are defined as follows. Matrices and vectors are represented by symbols in bold; $(\cdot)^T$ and $(\cdot)^H$ denote the transpose and conjugate transpose, respectively, $\mathbf{I}_{N_R}$ denotes the $N_R \times N_R$ identity matrix, and trace$\{\cdot\}$ is the trace of a square matrix.

2. Downlink Channel Model in Massive MIMO System

Let us consider a TDD-based Massive MIMO system with N_T antennas at the BS to simultaneously serve K users as illustrated in Figure 1. Each user is equipped with N_u antennas. Let N_R be the total number of antennas for the K users, then we have $N_R = K N_u$.

Let $\mathbf{x}_u \in \mathbb{C}^{N_u \times 1}, u = 1, \ldots, K$, represent the transmitted signal vector for the uth user. The received signal at the uth user, $\mathbf{y}_u \in \mathbb{C}^{N_u \times 1}$, can be expressed as follows:

$$
\begin{aligned}
\mathbf{y}_u &= \mathbf{H}_u \sum_{k=1}^{K} \mathbf{W}_k \mathbf{x}_k + \mathbf{n}_u \\
&= \mathbf{H}_u \mathbf{W}_u \mathbf{x}_u + \sum_{k=1, k \neq u}^{K} \mathbf{H}_u \mathbf{W}_k \mathbf{x}_k + \mathbf{n}_u,
\end{aligned}
\tag{1}
$$

where $\mathbf{H}_u \in \mathbb{C}^{N_u \times N_T}$, $\mathbf{W}_u \in \mathbb{C}^{N_T \times N_u}$, and $\mathbf{n}_u \in \mathbb{C}^{N_u \times 1}$ are the channel matrix from the BS to the uth user, the precoding matrix, and the noise vector for the uth user, respectively. The entries of the channel matrix are assumed to be identical independent distributed (i.i.d) random variables with zero mean and unit variance.

Let $\mathbf{y} = \begin{bmatrix} \mathbf{y}_1^T & \mathbf{y}_1^T & \cdots & \mathbf{y}_K^T \end{bmatrix}^T \in \mathbb{C}^{N_R \times 1}$ be the overall received signal vector for all users. Then, based on (1), $\mathbf{y}$ is given by

$$
\mathbf{y} = \mathbf{H}\mathbf{W}\mathbf{x} + \mathbf{n},
\tag{2}
$$

where $\mathbf{W} \in \mathbb{C}^{N_T \times N_R}$ is the precoding matrix for all users, $\mathbf{x} = \begin{bmatrix} \mathbf{x}_1^T & \mathbf{x}_2^T & \cdots & \mathbf{x}_K^T \end{bmatrix}^T$ is the transmitted signal vector for K users, and $\mathbf{n} \in \mathbb{C}^{N_R \times 1}$ is the noise vector at the K users. The entries of $\mathbf{n}$ are assumed to be identical independent
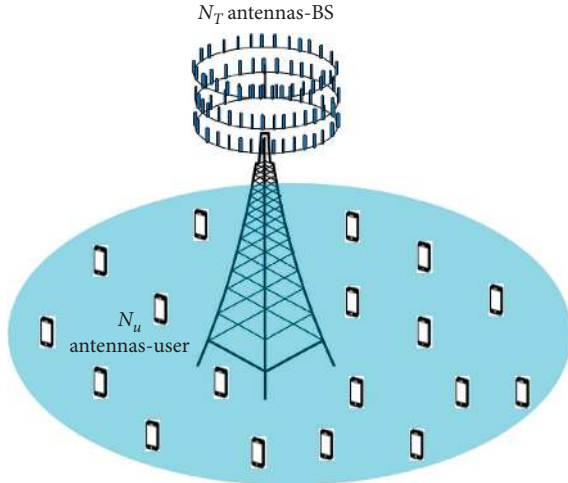
FIGURE 1: The downlink channel model in the Massive MIMO system.

distributed (i.i.d) random variables with zero mean and variance σ_n^2.

In reality, it is almost impossible for the BS to fully get the CSI due to the effects of thermal noise and pilot contamination. In other words, the system has to operate under imperfect CSI conditions. The accuracy of the CSI available at the BS side depends on the channel estimators to be used. The imperfect channel matrix $\mathbf{H} = \begin{bmatrix} \mathbf{H}_1^T & \mathbf{H}_2^T & \cdots & \mathbf{H}_K^T \end{bmatrix}^T \in \mathbb{C}^{N_R \times N_T}$ obtained by using the MMSE channel estimation can be modeled as follows [17, 18]:

$$\mathbf{H} = \sqrt{1 - \phi^2}\widetilde{\mathbf{H}} + \phi\mathbf{E}_{\mathrm{err}}, \tag{3}$$

where $\widetilde{\mathbf{H}} = \begin{bmatrix} \widetilde{\mathbf{H}}_1^T & \widetilde{\mathbf{H}}_2^T & \cdots & \widetilde{\mathbf{H}}_K^T \end{bmatrix}^T \in \mathbb{C}^{N_R \times N_T}$ is the perfect Rayleigh fading channel from the BS to all users in which entries $\widetilde{h}_{ij}$ are assumed to be complex Gaussian random variables with zero mean and unit variance. $\mathbf{E}_{\mathrm{err}} \in \mathbb{C}^{N_R \times N_T}$ is the channel estimation error matrix in which entries are assumed to be normalized i.i.d zero mean complex Gaussian random variables. $\phi \in [0, 1]$ is a parameter that indicates the accuracy of the channel estimator. From (3), we can see that $\phi = 0$ means that there is no channel estimation error and the CSI at the BS is perfect. Conversely, $\phi = 1$ indicates a complete failure of the channel estimator.

3. Review of the Principal Component Analysis Technique

The Principal Component Analysis technique was presented in [16, 19–21]. It is a mathematical tool that uses an orthogonal transformation to convert a set of observations of possibly correlated variables into a set of values of linearly uncorrelated variables, which are called principal components. Let $\mathbf{U} \in \mathbb{C}^{M \times N}$ be the original data set and $\mathbf{Y} \in \mathbb{C}^{M \times N}$ be the rerepresentation of that data set. Based on the eigenvalue decomposition of $\mathbf{U}\mathbf{U}^T$ in linear algebra, the relationship between $\mathbf{Y}$ and $\mathbf{U}$ is given by [16, 19]

$$\mathbf{Y} = \mathbf{B}\mathbf{U}. \tag{4}$$

Herein, $\mathbf{B} \in \mathbb{C}^{M \times M}$ denotes the principal components of $\mathbf{U}$. Then, (4) can be represented as follows:

$$\begin{bmatrix} \mathbf{y}_1 & \mathbf{y}_2 & \cdots & \mathbf{y}_N \end{bmatrix} = \begin{bmatrix} \mathbf{b}_1 \\ \mathbf{b}_2 \\ \vdots \\ \mathbf{b}_M \end{bmatrix} \begin{bmatrix} \mathbf{u}_1 & \mathbf{u}_2 & \cdots & \mathbf{u}_N \end{bmatrix}, \tag{5}$$

where $\mathbf{b}_i \in \mathbb{C}^{1 \times M}$ $(i = 1, 2, \ldots, M)$ is the row of $\mathbf{B}$, which is basic vectors correspond to eigenvectors of covariance matrix $\mathbf{U}\mathbf{U}^T$ for representing the columns of $\mathbf{U}$. The $\mathbf{B}$ matrix is defined in such a way that the first principal component $\mathbf{b}_1$ has the largest variance, each succeeding component in turn has the highest variance under the constraint that it is orthogonal to the previous components.

According to [16, 19, 20], the PCA technique based on the eigenvalue decomposition of $\mathbf{U}\mathbf{U}^T$ is summarized as follows.

First, each row of $\mathbf{U}$ is normalized to have zero mean as follows:

$$\widetilde{\mathbf{U}} = \mathbf{U} - \mathbf{U}_{\mathrm{mean}}, \tag{6}$$

where $\mathbf{U}_{\mathrm{mean}} \in \mathbb{C}^{M \times N}$ represents the mean of rows of the matrix $\mathbf{U}$. Defining $\mathbf{v}_k = (\mathbf{v}_1, \mathbf{v}_2, \ldots, \mathbf{v}_m) \in \mathbb{C}^{M \times 1}$ as the set of eigenvectors associated with the eigenvalues μ_k of the symmetric matrix $\widetilde{\mathbf{U}}\widetilde{\mathbf{U}}^T$, then we have

$$\left(\widetilde{\mathbf{U}}\widetilde{\mathbf{U}}^T\right)\mathbf{v}_k = \mu_k\mathbf{v}_k, \tag{7}$$

where $\mu_k = (\mu_1, \mu_2, \ldots, \mu_m) \in \mathbb{R}^{M \times 1}$. Applying the QR decomposition to $\widetilde{\mathbf{U}}$, we obtain

$$\widetilde{\mathbf{U}} = \mathbf{Q}\mathbf{R}, \tag{8}$$

where $\mathbf{R} \in \mathbb{C}^{M \times N}$ is an upper triangular matrix and $\mathbf{Q} \in \mathbb{C}^{M \times M}$ is a unitary matrix. Therefore, we can write

$$\widetilde{\mathbf{U}}\widetilde{\mathbf{U}}^T = \mathbf{Q}\mathbf{R}(\mathbf{Q}\mathbf{R})^T. \tag{9}$$

By using the SVD decomposition, the $\mathbf{R}^H$ matrix can be expressed as follows:

$$\mathbf{R}^H = \mathbf{U}\mathbf{\Sigma}\mathbf{V}^H. \tag{10}$$

From (9) and (10), it follows that

$$\widetilde{\mathbf{U}}\widetilde{\mathbf{U}}^T = \mathbf{Q}\left(\mathbf{U}\mathbf{\Sigma}\mathbf{V}^H\right)^T\left(\mathbf{U}\mathbf{\Sigma}\mathbf{V}^T\right)\mathbf{Q}^T = \mathbf{Q}\mathbf{V}\mathbf{\Sigma}^2\left(\mathbf{Q}\mathbf{V}\right)^T. \tag{11}$$

Or equivalently, we have

$$\left(\widetilde{\mathbf{U}}\widetilde{\mathbf{U}}^T\right)(\mathbf{Q}\mathbf{V}) = (\mathbf{Q}\mathbf{V})\mathbf{\Sigma}^2. \tag{12}$$

From (7) and (12), we can see that the eigenvectors and eigenvalues of the covariance matrix $(\widetilde{\mathbf{U}}\widetilde{\mathbf{U}}^T)$ are contained in the matrices $\mathbf{Q}\mathbf{V}$ and $\mathbf{\Sigma}^2$, respectively. Therefore, the principal component matrix $\mathbf{B}$ is given by

$$\mathbf{B} = \mathbf{Q}\mathbf{V}. \tag{13}$$

4. Proposed Precoder

4.1. Proposed PCA-LP Precoder. In this section, we construct a linear precoding algorithm based on the principal component analysis technique, called PCA-LP precoder. In our proposal, the precoding matrix is given by

$$\mathbf{W}_{\mathrm{PCA\_LP}} = \beta \mathbf{W}_a \mathbf{W}_b, \tag{14}$$

where $\mathbf{W}_a \in \mathbb{C}^{N_T \times N_R}$, $\mathbf{W}_b \in \mathbb{C}^{N_R \times N_R}$, and β is the normalized power factor, which is given by

$$\beta = \sqrt{\frac{N_R}{\mathrm{trace}\left(\mathbf{W}_{\mathrm{PCA\_LP}} \mathbf{W}_{\mathrm{PCA\_LP}}^H\right)}}. \tag{15}$$

The first precoding matrix $\mathbf{W}_a$ is obtained using the conventional MMSE technique as follows:

$$\begin{aligned} \mathbf{W}_a &= \mathbf{H}^H \left(\mathbf{H}\mathbf{H}^H + \sigma^2 \mathbf{I}_{N_R}\right)^{-1} \\ &= \left[\mathbf{W}_a^1, \mathbf{W}_a^2, \ldots, \mathbf{W}_a^K\right], \end{aligned} \tag{16}$$

where $\sigma^2 = \sigma_n^2 / E_s$, E_s is the transmit symbol energy, and $\mathbf{W}_a^k \in \mathbb{C}^{N_T \times N_u}$ $(k = 1, 2, \ldots, K)$ is the precoding matrix for the kth user.

The second precoding matrix $\mathbf{W}_b$ is constructed based on the PCA transformation as follows.

First, using $\mathbf{W}_a^k$ in (16), the effective channel matrix for the kth user is computed to be

$$\mathbf{H}_{\mathrm{eff}}^k = \mathbf{H}_k \mathbf{W}_a^k, \tag{17}$$

where $\mathbf{H}_k \in \mathbb{C}^{N_u \times N_T}$ is the channel matrix from BS to the kth user.

Next, the channel matrix $\mathbf{H}_{\mathrm{eff}}^k$ is normalized to give $\mathbf{H}_{\mathrm{nor}}^k \in \mathbb{C}^{N_u \times N_u}$ with zero mean as follows:

$$\mathbf{H}_{\mathrm{nor}}^k = \mathbf{H}_{\mathrm{eff}}^k - \mathbf{H}_{\mathrm{mean}}^k, \tag{18}$$

where $\mathbf{H}_{\mathrm{mean}}^k \in \mathbb{C}^{N_u \times N_u}$ denotes the mean matrix, whose entries are the means of the rows of the matrix $\mathbf{H}_{\mathrm{eff}}^k$.

Applying the QR decomposition to $\mathbf{H}_{\mathrm{nor}}^k$, we obtain

$$\mathbf{H}_{\mathrm{nor}}^k = \mathbf{Q}_{\mathrm{nor}}^k \mathbf{R}_{\mathrm{nor}}^k, \tag{19}$$

where $\mathbf{R}_{\mathrm{nor}}^k \in \mathbb{C}^{N_u \times N_u}$ is an upper triangular matrix and $\mathbf{Q}_{\mathrm{nor}}^k \in \mathbb{C}^{N_u \times N_u}$ is a unitary matrix with orthogonal columns.

After that, the SVD operation is applied to $(\mathbf{R}_{\mathrm{nor}}^k)^H$ to give

$$\left(\mathbf{R}_{\mathrm{nor}}^k\right)^H = \mathbf{U}_{\mathrm{nor}}^k \boldsymbol{\Sigma}_{\mathrm{nor}}^k \left(\mathbf{V}_{\mathrm{nor}}^k\right)^H, \tag{20}$$

where $\mathbf{U}_{\mathrm{nor}}^k \in \mathbb{C}^{N_u \times N_u}$ and $\mathbf{V}_{\mathrm{nor}}^k \in \mathbb{C}^{N_u \times N_u}$ are unitary matrices with orthogonal columns and $\boldsymbol{\Sigma}_{\mathrm{nor}}^k \in \mathbb{R}^{N_u \times N_u}$ is a diagonal matrix.

The principal component factor matrix $\mathbf{A}_{\mathrm{PCA}}^k \in \mathbb{C}^{N_u \times N_u}$ for the kth user is obtained as

$$\mathbf{A}_{\mathrm{PCA}}^k = \mathbf{Q}_{\mathrm{nor}}^k \mathbf{V}_{\mathrm{nor}}^k. \tag{21}$$

Using $\mathbf{A}_{\mathrm{PCA}}^k$ and $\mathbf{H}_{\mathrm{eff}}^k$, the combination channel matrix $\mathbf{H}_{\mathrm{com}}^k \in \mathbb{C}^{N_u \times N_u}$ for the kth user is computed as follows:

$$\mathbf{H}_{\mathrm{com}}^k = \mathbf{A}_{\mathrm{PCA}}^k \mathbf{H}_{\mathrm{eff}}^k. \tag{22}$$

From (22), the precoding matrix $\mathbf{W}_b^k \in \mathbb{C}^{N_u \times N_u}$ for the kth user based on the conventional ZF algorithm is given by

$$\mathbf{W}_b^k = \left(\mathbf{H}_{\mathrm{com}}^k\right)^H \left[\mathbf{H}_{\mathrm{com}}^k \left(\mathbf{H}_{\mathrm{com}}^k\right)^H\right]^{-1}. \tag{23}$$

Finally, the second precoding matrix $\mathbf{W}_b$ and the principal component factor matrix $\mathbf{A}_{\mathrm{PCA}} \in \mathbb{C}^{N_R \times N_R}$ for all users are represented as follows:

$$\mathbf{W}_b = \begin{bmatrix} \mathbf{W}_b^1 & 0 & & 0 \\ 0 & \mathbf{W}_b^2 & & 0 \\ \vdots & \vdots & \ddots & \vdots \\ 0 & 0 & & \mathbf{W}_b^K \end{bmatrix}, \tag{24}$$

$$\mathbf{A}_{\mathrm{PCA}} = \begin{bmatrix} \mathbf{A}_{\mathrm{PCA}}^1 & 0 & & 0 \\ 0 & \mathbf{A}_{\mathrm{PCA}}^2 & & 0 \\ \vdots & \vdots & \ddots & \vdots \\ 0 & 0 & & \mathbf{A}_{\mathrm{PCA}}^K \end{bmatrix}. \tag{25}$$

The proposed algorithm PCA-LP is summarized in Algorithm 1.

At the user side, the received signal vector for all users can be expressed as

$$\mathbf{y} = \mathbf{H} \mathbf{W}_{\mathrm{PCA\_LP}} \mathbf{x} + \mathbf{n}. \tag{26}$$

Using $\mathbf{y}$ in (26), the estimated signal vector is given by

$$\widehat{\mathbf{x}} = \frac{\mathbf{A}_{\mathrm{PCA}} \mathbf{y}}{\beta} = \mathbf{A}_{\mathrm{PCA}} \left[\frac{\left(\mathbf{H} \mathbf{W}_{\mathrm{PCA\_LP}} \mathbf{x} + \mathbf{n}\right)}{\beta}\right]. \tag{27}$$

From (27), with $\mathbf{W}_{\mathrm{PCA}} = \mathbf{W}_a \mathbf{W}_b$, the error covariance matrix can be obtained as

$$\begin{aligned} \mathbf{Q} &= E\left\{\mathrm{trace}\left[(\widehat{\mathbf{x}} - \mathbf{x})(\widehat{\mathbf{x}} - \mathbf{x})^H\right]\right\} \\ &= \mathrm{trace}\left\{E_s\left(\mathbf{A}_{\mathrm{PCA}} \mathbf{H} \mathbf{W}_{\mathrm{PCA}} - \mathbf{I}_{N_R}\right)\left(\mathbf{A}_{\mathrm{PCA}} \mathbf{H} \mathbf{W}_{\mathrm{PCA}} - \mathbf{I}_{N_R}\right)^H \right. \\ &\quad \left. + \frac{\sigma_n^2 \mathbf{A}_{\mathrm{PCA}} \mathbf{A}_{\mathrm{PCA}}^H}{\beta^2}\right\}. \end{aligned} \tag{28}$$

The Empirical Cumulative Distribution Functions (ECDFs) of the maximum diagonal element of $\mathbf{Q}$ in (28) for the PCA-LP and PCA-MMSE-BD precoders at different accuracy levels of the channel estimator are illustrated in Figure 2. It can be observed from the figure that the largest elements on the diagonals of the error covariance matrices for both precoders increase as the channel estimation error increases. In addition, the PCA-MMSE-BD precoder provides slightly smaller maximum errors than the PCA-LP one in all cases.

Figure 3 shows the ECDFs of the sums of diagonal elements of the error covariance matrices for the PCA-MMSE-BD precoder and the proposed PCA-LP precoder. As can be seen from the figure, the sums of the diagonal elements for all the precoders experience exactly the same behavior as the

(1) **Input**: $N_T, N_R, \mathbf{H}$.
(2) Generate the matrix $\mathbf{W}_a = [\mathbf{W}_a^1, \mathbf{W}_a^2, \ldots, \mathbf{W}_a^K]$ as in (16).
(3) Compute the matrices $\mathbf{H}_{\text{eff}}^k = \mathbf{H}_k \mathbf{W}_a^k$ and $\mathbf{H}_{\text{nor}}^k = \mathbf{H}_{\text{eff}}^k - \mathbf{H}_{\text{mean}}^k$.
(4) Apply QR decomposition to $\mathbf{H}_{\text{nor}}^k$: $\mathbf{H}_{\text{nor}}^k = \mathbf{Q}_{\text{nor}}^k \mathbf{R}_{\text{nor}}^k$.
(5) Apply the SVD to $(\mathbf{R}_{\text{nor}}^k)^H$: $(\mathbf{R}_{\text{nor}}^k)^H = \mathbf{U}_{\text{nor}}^k \mathbf{\Sigma}_{\text{nor}}^k (\mathbf{V}_{\text{nor}}^k)^H$.
(6) Create the matrices $\mathbf{A}_{\text{PCA}}^k = \mathbf{Q}_{\text{nor}}^k \mathbf{V}_{\text{nor}}^k$ and $\mathbf{H}_{\text{com}}^k = \mathbf{A}_{\text{PCA}}^k \mathbf{H}_{\text{eff}}^k$.
(7) Generate the precoding matrix $\mathbf{W}_b^k = (\mathbf{H}_{\text{com}}^k)^H [\mathbf{H}_{\text{com}}^k (\mathbf{H}_{\text{com}}^k)^H]^{-1}$.
(8) Repeat Step 3 to Step 7 until the precoding matrices $\mathbf{W}_b^k$ for all users are obtained.
(9) Create the matrices $\mathbf{W}_b$ and $\mathbf{A}_{\text{PCA}}$ by arranging $\mathbf{W}_b^k$ and $\mathbf{A}_{\text{PCA}}^k$ to the main diagonals of $\mathbf{W}_b$ and $\mathbf{A}_{\text{PCA}}$ as in (24) and (25), respectively.
(10) **Output**: $\mathbf{W}_a = [\mathbf{W}_a^1, \mathbf{W}_a^2, \ldots, \mathbf{W}_a^K]$, $\mathbf{W}_b = \text{diag}(\mathbf{W}_b^1, \mathbf{W}_b^2, \ldots, \mathbf{W}_b^K)$, $\mathbf{A}_{\text{PCA}} = \text{diag}(\mathbf{A}_{\text{PCA}}^1, \mathbf{A}_{\text{PCA}}^2, \ldots, \mathbf{A}_{\text{PCA}}^K)$,
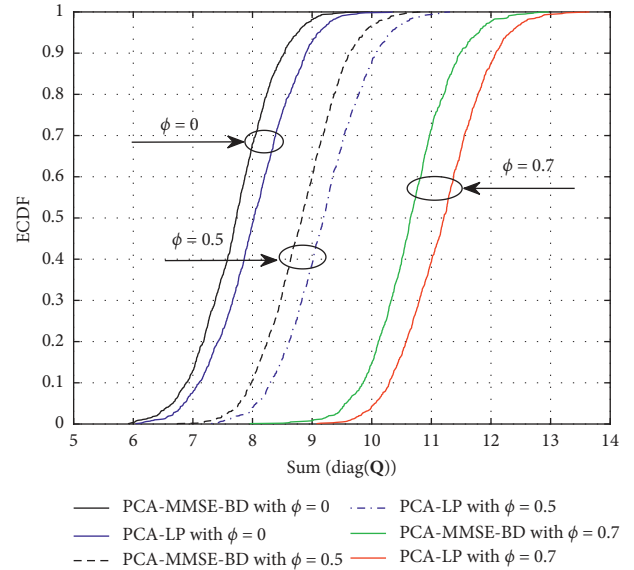$\beta = \sqrt{N_R / \text{trace}(\mathbf{W}_{\text{PCA\_LP}} \mathbf{W}_{\text{PCA\_LP}}^H)}$.

ALGORITHM 1: The PCA-LP precoding algorithm.
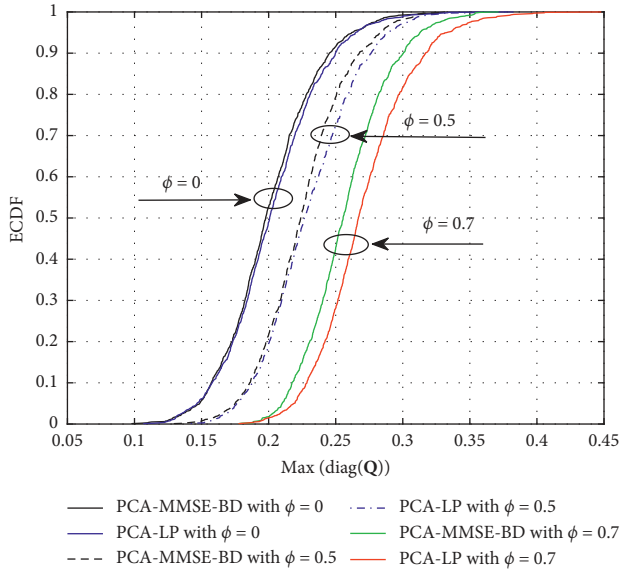
FIGURE 2: Empirical CDF of the maximum of diagonal elements of $\mathbf{Q}$ for $N_T = 64$, $N_u = 2$, and $K = 32$.

FIGURE 3: Empirical CDF of the sum of diagonal elements of $\mathbf{Q}$ for $N_T = 64$, $N_u = 2$, and $K = 32$.

maximum diagonal elements. Similar to the results in Figure 2, the mean square errors for both precoders increase when the channel estimation error increases. Besides, the PCA-MMSE-BD precoder provides slightly smaller summation errors than the PCA-LP one in all cases.

Since the diagonal elements of error covariance matrices determine the mean square errors (MSEs) between the transmitted symbols and the recovered ones, BER performances of the PCA-MMSE-BD and the proposed PCA-LP precoders decrease as the channel estimation error increases. Fortunately, the slightly higher MSE of the proposed precoder does not incur significant BER performance degradation as compared to the PCA-MMSE-BD precoder.

4.2. Computational Complexity Analysis. In this section, the computational complexity of the proposed PCA-LP precoder is evaluated and compared with those of the

LC-RBD-LR-ZF in [15] and the PCA-MMSE-BD in [16]. The complexities are evaluated by counting the necessary floating point operations (flops). We assume that each real operation (an addition, a multiplication, or a division) is counted as a flop. Hence, a complex multiplication and a division is equal to 6 flops and 11 flops, respectively. It is worth noting that the QR decomposition of an $m \times n$ complex matrix requires $6mn^2 + 4mn - n^2 - n$ flops. According to [22], the SVD of a $m \times n$ $(m \geq n)$ complex matrix requires $(4m^2 n + 8mn^2 + 9n^3)$ flops. Based on the abovementioned assumptions, the computational complexity of the proposed algorithm PCA-LP is computed to be

$$F_{\text{PCA-LP}} = F_1 + F_2 + F_3 \text{ (flops)}, \tag{29}$$

where F_1 and F_2 are the number of flops to find the matrices $\mathbf{W}_a$ and $\mathbf{W}_b$ and F_3 is the number of flops for the multiplication two matrices $\mathbf{W}_a$ and $\mathbf{W}_b$.

TABLE 1: Computational complexity comparison.

Precoding algorithms	Complexity (flops)	Complexity level
LC – RBD – LR – ZF [15]	$K[6(N_R - N_u)(N_R + N_T - N_u)^2 + 4(N_R - N_u)(N_R + N_T - N_u) - (N_R + N_T - N_u)^2$ $- (N_R + N_T - N_u)] + K(8N_T^2 N_u - 2N_T N_u) + K(16N_u^2 N_T - 2N_u N_T + 8N_u^3 - 2N_u^2$ $+ F_{\text{update–LLL}}) + K(8N_u^3 + 16N_u^2 N_T - 2N_u^2 - 2N_u N_T) + 8KN_T^2 N_R - 2N_T N_R$	$\mathcal{O}(N_R^4)$
PCA – MMSE – BD [16]	$[8N_R^3 + 16N_R^2 N_T - N_R^2 - 2N_R N_T + N_R + 1] + K(6N_T^2 N_u + 4N_T N_u - N_u^2 - N_u)$ $+ K(8N_u^2 N_T - 2N_u^2) + K(24N_u^3 + 4N_u^2 - 2N_u) + 41KN_u^3 + K(8N_u^3 - 2N_u^2)$ $+ K(16N_u^3 - 4N_u^2) + K(56N_u^3 - 8N_u^2) + 8N_R^2 N_T - 2N_R^2$	$\mathcal{O}(N_T N_R^2)$
PCA – LP	$8N_R^3 + 16N_R^2 N_T - N_R^2 - 2N_R N_T + 1 + K(8N_u^2 N_T - 2N_u^2)$ $+ K(6N_u^3 + 3N_u^2 - N_u) + 21KN_u^3 + 2K(8N_u^3 - 2N_u^2) + K(24N_u^3 - 4N_u^2)$ $+ 8N_R^2 N_T - 2N_R^2$	$\mathcal{O}(N_T N_R^2)$

The number of flops to find the matrix $\mathbf{W}_a$ is equal to

$$F_1 = 8N_R^3 + 16N_R^2 N_T - N_R^2 - 2N_R N_T + N_R + 1 \,(\text{flops}). \tag{30}$$

The number of flops to find $\mathbf{W}_b$ is expressed as follows:

$$F_2 = F_4 + F_5 + F_6 + F_7 + F_8 + F_9 \,(\text{flops}), \tag{31}$$

where F_4 is the number of flops for the multiplication two matrices $\mathbf{H}_k$ and $\mathbf{W}_a^k$; F_5 is the number of flops for the QR decomposition of $\mathbf{H}_{\text{nor}}^k$; F_6 is the number of flops for SVD of $(\mathbf{R}_{\text{nor}}^k)^H$; F_7 is the number of flops for the multiplication two matrices $\mathbf{Q}_{\text{nor}}^k$ and $\mathbf{V}_{\text{nor}}^k$; F_8 is the number of flops of the multiplication two matrices $\mathbf{A}_{\text{PCA}}^k$ and $\mathbf{H}_{\text{eff}}^k$. Finally, F_9 is number of flops to find the matrices $\mathbf{W}_b^k$. These items are given by

$$\begin{aligned} F_4 &= K\left(8N_u^2 N_T - 2N_u^2\right)(\text{flops}), \\ F_5 &= K\left(6N_u^3 + 3N_u^2 - N_u\right)(\text{flops}), \\ F_6 &= 21KN_u^3 \,(\text{flops}), \\ F_7 &= K\left(8N_u^3 - 2N_u^2\right)(\text{flops}), \\ F_8 &= K\left(8N_u^3 - 2N_u^2\right)(\text{flops}), \\ F_9 &= K\left(24N_u^3 - 4N_u^2\right)(\text{flops}). \end{aligned} \tag{32}$$

Besides, F_3 is calculated as

$$F_3 = 8N_R^2 N_T - 2N_R^2 \,(\text{flops}). \tag{33}$$

Therefore, the number of flops for the proposed PCA-LP precoder is represented as follows:

$$\begin{aligned} F_{\text{PCA–LP}} &= F_1 + F_2 + F_3 \\ &= 8N_R^3 + 16N_R^2 N_T - N_R^2 - 2N_R N_T + 1 \\ &+ K\left(8N_u^2 N_T - 2N_u^2\right) + K\left(6N_u^3 + 3N_u^2 - N_u\right) \\ &+ 21KN_u^3 + 2K\left(8N_u^3 - 2N_u^2\right) + K\left(24N_u^3 - 4N_u^2\right) \\ &+ 8N_R^2 N_T - 2N_R^2 \,(\text{flops}) \\ &\sim \mathcal{O}\left(N_T N_R^2\right). \end{aligned} \tag{34}$$
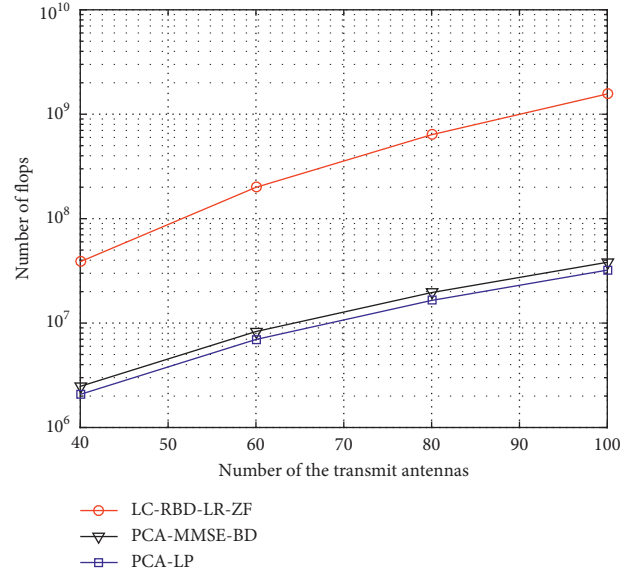

FIGURE 4: Comparison of the complexity of the proposed precoding algorithm with the LC-RBD-LR-ZF and PCA-MMSE-BD algorithms.

Using similar complexity analysis steps, we are able to obtain the complexities of both the LC-RBD-LR-ZF and the PCA-MMSE-BD precoders, which are summarized in Table 1 in the next page.

5. Simulation Results

In this section, we compare both the computational complexity and the system performance of the proposed PCA-LP precoder with those of its LC-RBD-LR-ZF and PCA-MMSE-BD counterparts.

Figure 4 demonstrates the computational complexities of the PCA-LP, LC-RBD-LR-ZF, and PCA-MMSE-BD precoders. In this scenario, $N_T = N_R$ is varied from 40 to 100 transmit antennas, $N_u = 2$, and $K = N_R/2$. Numerical results show that the computational complexity of the proposed PCA-LP precoder is significantly lower than the complexity of the LC-RBD-LR-ZF precoder and lower than that of the PCA-MMSE-BD precoder. For example, at $N_R = N_T = 80$ antennas, the complexity of the proposed PCA-LP
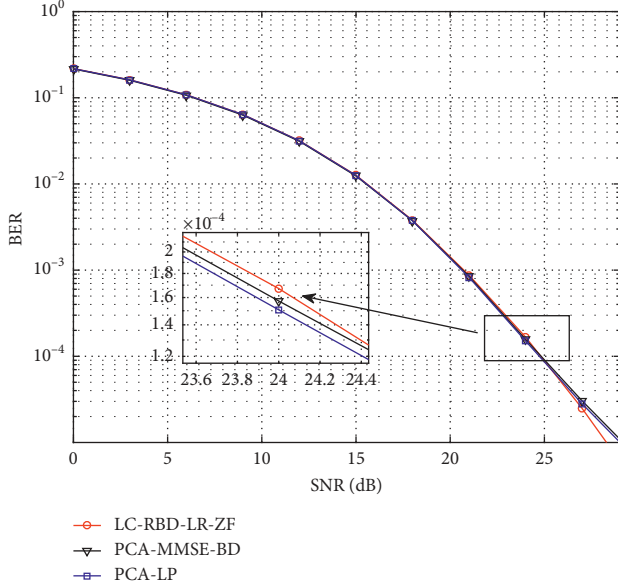
FIGURE 5: The system performance with $N_T = N_R = 64$, $K = 32$, $N_u = 2$ in the perfect CSI condition at the BS side.
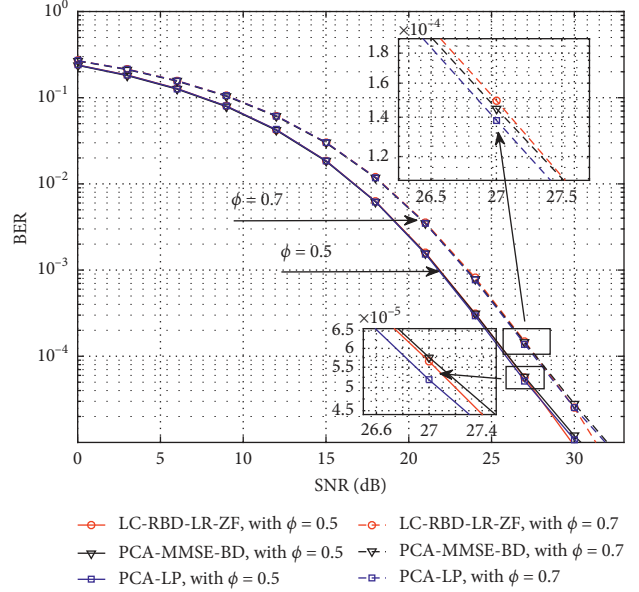

FIGURE 6: The system performance with $N_T = N_R = 64$, $K = 32$, $N_u = 2$, $\phi = 0.5$, and $\phi = 0.7$ in the imperfect CSI condition at the BS side.
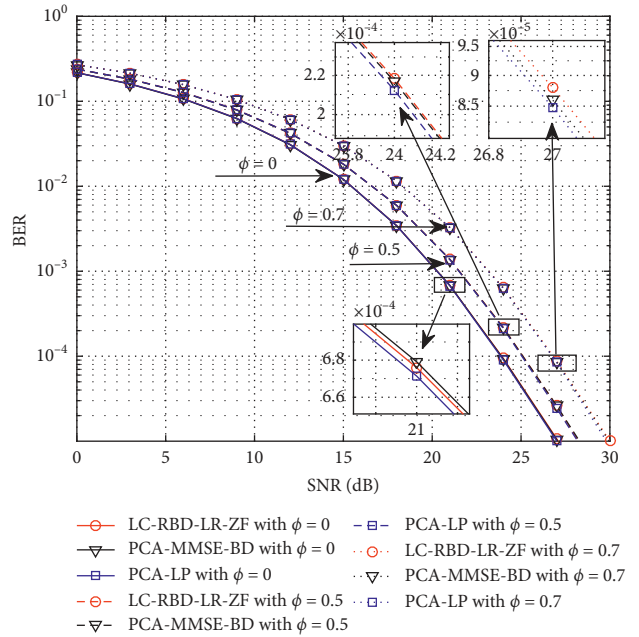

FIGURE 7: The system performance with $N_T = N_R = 128$, $K = 64$, and $N_u = 2$ in the perfect and imperfect CSI conditions at the BS side.

precoder is approximately equal to 2.58% and 84.07% of the complexities of the LC-RBD-LR-ZF and PCA-MMSE-BD precoders, respectively. We can see that the complexity of the LC-RBD-LR-ZF precoder is very large for two reasons: firstly, the number of the QR operations applied to the extended channel matrix is too large. Secondly, the sizes of the precoding matrices $\mathbf{P}^a \in \mathbb{C}^{N_T \times K N_T}$ and $\widetilde{\mathbf{P}}^b \in \mathbb{C}^{K N_T \times N_R}$ increase proportionally to N_R and N_T. Therefore, the number of flops required for the multiplications of the two matrices $\mathbf{P}^a$ and $\widetilde{\mathbf{P}}^b$ also increase.

The BER curves of the proposed PCA-LP as well as those of the LC-RBD-LR-ZF and PCA-MMSE-BD precoders are illustrated in Figures 5–8. In Figure 5, the system is assumed to work in the perfect CSI condition (i.e., $\phi = 0$ and $\mathbf{H} = \widetilde{H}$) with the following parameters: $N_R = N_T = 64$, $N_u = 2$, $K = N_R/2$, and 4-QAM modulation. It can be seen from Figure 5 that the BER curves of the three precoders are almost identical when the $SNR \leq 27$ dB. For larger SNR, the LC-RBD-LR-ZF precoder outperforms the remaining ones.

In Figure 6, we simulate the system performance in the imperfect CSI condition (i.e., $\mathbf{H} = \sqrt{1 - \phi^2} \widetilde{\mathbf{H}} + \phi \mathbf{E}_{\text{err}}$) for $\phi = 0.5$ and $\phi = 0.7$. Other parameters are the same as those used to generate Figure 5. Similar to the results in Figure 5, the results in Figure 6 show that the three precoders provide nearly the same system performance. As the SNR is sufficiently large, the LC-RBD-LR-ZF precoder is able to provide better BER performance. The results from Figures 4–6 show that the LC-RBD-LR-ZF precoder can marginally outperform the proposed PCA-LP and PCA-MMSE-BD precoders in the sufficiently large SNR regions. However, it suffers from noticeably higher computational complexities.

In Figure 7, the BER performances of the system with $N_T = 128$, $N_u = 2$, and $K = 64$ are illustrated for the three precoders in the perfect and imperfect CSI conditions at the

BS side. Here, 4-QAM modulation is also adopted. The simulation results in Figure 7 show that the BER curves of the PCA-LP proposed precoder almost coincide with those of the remaining precoders in all scenarios. Moreover, one can observe from Figures 5–7 that as N_T increases from 64 to 128, the LC-RBD-LR-ZF precoder no longer outperforms the proposed PCA-LP one in the high SNR regions. Clearly, the larger N_T is deployed at the BS, the better
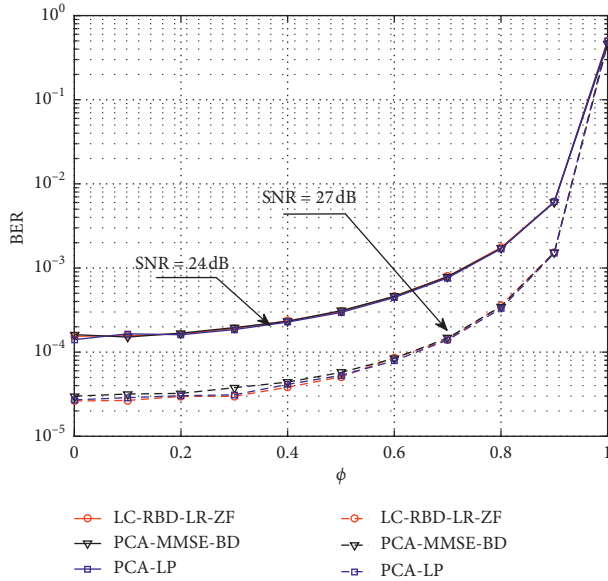
FIGURE 8: The system performance according to ϕ at SNR = 24 dB and 27 dB with $N_T = N_R = 64$, $K = 32$, and $N_u = 2$.

system performance the proposed PCA-LP precoder can achieve.

Figure 8 illustrates the BER curves of the three precoders as functions of ϕ at SNR = 24 dB and 27 dB. Other simulation parameters are kept the same as the ones used for Figure 5, i.e., $N_T = N_R = 64$, $K = 32$, $N_u = 2$, and 4-QAM modulation. We again see that for the same parameters, the three precoders provide nearly the same BERs, particularly when ϕ becomes larger. Furthermore, the channel estimation error has an adverse effect on the system performance no matter which precoder is employed. The larger values of ϕ make the system performance deteriorate more rapidly.

It is noteworthy that the simulation results in Figures 5–8 are obtained for the worst cases when $N_T = K \times N_u$, i.e., when the systems work in full-load conditions. As the number of user gets smaller, the system performance definitely becomes better.

6. Conclusions

This paper proposes the PCA-LP precoder with low complexity in Massive MIMO systems with imperfect CSI at the BS side. The proposed precoder consists of two component. The first one is designed to eliminate interference from neighboring users and the second one is created based on the Principal Component Analysis technique and the linear precoding algorithm to improve the system performance. Numerical and simulation results show that the computational complexity of the proposed PCA-LP precoder is significantly lower than the complexity of the LC-RBD-LR-ZF precoder and lower than that of the PCA-MMSE-BD precoder, while they all provide nearly the same system performance in all simulation scenarios. Simulation results also show that the channel estimation error has an adverse effect on the system performance no matter which precoder is adopted. For all precoders, the system performance

decreases as the channel estimation error increases and vice versa. Moreover, the larger the channel estimation error is, the more rapidly the system performance deteriorates. Taking both system performance and complexity into consideration, the proposed PCA-LP precoder can be a potential digital beamforming technique for the downlinks of Massive MIMO systems.

Data Availability

All results included in this paper are generated by simulation in Matlab.

Conflicts of Interest

The authors declare that they have no conflicts of interest.

References

[1] H. Q. Ngo, *Massive MIMO: Fundamentals and System Designs*, Vol. 1642, Linköping University Electronic Press, Linköping, Sweden, 2015.

[2] L. Lu, G. Y. Li, A. L. Swindlehurst, A. Ashikhmin, and R. Zhang, "An overview of massive mimo: benefits and challenges," *IEEE Journal of Selected Topics in Signal Processing*, vol. 8, no. 5, pp. 742–758, 2014.

[3] T. L. Marzetta, "Noncooperative cellular wireless with unlimited numbers of base station antennas," *IEEE Transactions on Wireless Communications*, vol. 9, no. 11, pp. 3590–3600, 2010.

[4] T. L. Marzetta, "Massive MIMO: an introduction," *Bell Labs Technical Journal*, vol. 20, pp. 11–22, 2015.

[5] H. Y. T. L. Marzetta, E. G. Larsson, and H. Q. Ngo, *Fundamentals of Massive MIMO*, Cambridge University Press, Cambridge, UK, 2016.

[6] E. G. Larsson, O. Edfors, F. Tufvesson, and T. L. Marzetta, "Massive MIMO for next generationC wireless systems," *IEEE Communications Magazine*, vol. 52, no. 2, pp. 186–195, 2014.

[7] V. P. Selvan, M. S. Iqbal, and H. S. Al-Raweshidy, "Performance analysis of linear precoding schemes for very large multi-user MIMO downlink system," in *Proceedings of the Fourth Edition of the International Conference on the Innovative Computing Technology (INTECH 2014)*, pp. 219–224, London, UK, 2014.

[8] H. Q. Ngo, E. G. Larsson, and T. L. Marzetta, "Massive MU-MIMO downlink TDD systems with linear precoding and downlink pilots," in *Proceedings of the 51st Annual Allerton Conference on Communication, Control, and Computing (Allerton)*, pp. 293–298, Monticello, IL, USA, 2013.

[9] Y. S. Cho, J. Kim, W. Y. Yang, and C. G. Kang, *MIMO-OFDM Wireless Communications with MATLAB*, John Wiley & Sons, Hoboken, NJ, USA, 2010.

[10] Q. H. Spencer, A. L. Swindlehurst, and M. Haardt, "Zero-forcing methods for downlink spatial multiplexing in multiuser mimo channels," *IEEE Transactions on Signal Processing*, vol. 52, no. 2, pp. 461–471, 2004.

[11] J. Wu, S. Fang, L. Li, and Y. Yang, "QR decomposition and gram Schmidt orthogonalization based low-complexity multi-user MIMO precoding," in *Proceedings of the 10th International Conference on Wireless Communications, Networking and Mobile Computing (WiCOM 2014)*, pp. 61–66, Beijing, China, September 2014.

[12] W. Li and M. Latva-aho, "An efficient channel block diago-nalization method for generalized zero forcing assisted mimo broadcasting systems," *IEEE Transactions on Wireless Communications*, vol. 10, no. 3, pp. 739–744, March 2011.

[13] H. Wang, L. Li, L. Song, and X. Gao, "A linear precoding scheme for downlink multiuser mimo precoding systems," *IEEE Communications Letters*, vol. 15, no. 6, pp. 653–655, 2011.

[14] V. Stankovic and M. Haardt, "Generalized design of multi-user mimo precoding matrices," *IEEE Transactions on Wireless Communications*, vol. 7, no. 3, pp. 953–961, 2008.

[15] K. Zu and R. C. de Lamare, "Low-complexity lattice reduc-tion-aided regularized block diagonalization for mu-mimo systems," *IEEE Communications Letters*, vol. 16, no. 6, pp. 925–928, 2012.

[16] S. B. M. Priya and P. Kumar, "Design of low complex linear precoding scheme for mu-mimo systems," *Wireless Personal Communications*, vol. 97, no. 1, pp. 1097–1116, 2017.

[17] I. Frigyes, J. Bito, and P. Bakki, *Advances in Mobile and Wireless Communications: Views of the 16th IST Mobile and Wireless Communication Summit*, Springer, Berlin, Germany, 2008.

[18] F. Rusek, D. Persson, B. K. Buon Kiong Lau et al., "Scaling up MIMO: opportunities and challenges with very large arrays," *IEEE Signal Processing Magazine*, vol. 30, no. 1, pp. 40–60, 2013.

[19] A. Sharma, K. K. Paliwal, S. Imoto, and S. Miyano, "Principal component analysis using qr decomposition," *International Journal of Machine Learning and Cybernetics*, vol. 4, no. 6, pp. 679–683, 2013.

[20] J. Shlens, "A tutorial on principal component analysis," 2005, https://www.cs.cmu.edu/elaw/papers/pca.pdf.

[21] C. M. Bishop, *Pattern Recognition and Machine Learning*, Springer, Berlin, Germany, 2006.

[22] G. H. Golub and C. F. Van Loan, *Matrix Computations*, Johns Hopkins University Press, Baltimore, MD, USA, 1996.